



HAL
open science

Uptake of m -xylene and VOC emissions by mineral photocatalytic paints of indoor air building interest

Julien Morin, Gregory Brochard, Virgine Bergé, Aurélie Rosset, Sébastien Artous, Simon Clavaguera, Rafal Strekowski, Henri Wortham

► To cite this version:

Julien Morin, Gregory Brochard, Virgine Bergé, Aurélie Rosset, Sébastien Artous, et al.. Uptake of m -xylene and VOC emissions by mineral photocatalytic paints of indoor air building interest. *Environmental science.Nano*, 2023, 10.1039/d3en00084b . hal-04102042

HAL Id: hal-04102042

<https://amu.hal.science/hal-04102042>

Submitted on 22 May 2023

HAL is a multi-disciplinary open access archive for the deposit and dissemination of scientific research documents, whether they are published or not. The documents may come from teaching and research institutions in France or abroad, or from public or private research centers.

L'archive ouverte pluridisciplinaire **HAL**, est destinée au dépôt et à la diffusion de documents scientifiques de niveau recherche, publiés ou non, émanant des établissements d'enseignement et de recherche français ou étrangers, des laboratoires publics ou privés.

Copyright

1 **Uptake of m-xylene and VOC emissions by mineral photocatalytic paints of**
2 **indoor air building interest**

3 Julien Morin^a, Gregory Brochard^b, Virgine Bergé^b, Aurélie Rosset^c, Sébastien Artous^c, Simon
4 Clavaguera^c, Rafal S. Strekowski^{a,d}, Henri Wortham^{*,a}

5 ^a Aix Marseille Univ, CNRS, LCE, Marseille, France

6 ^b ALLIOS, 185 chemin de St Lambert, 13821 La penne sur Huveaune, France

7 ^c Univ. Grenoble Alpes, CEA, LITEN, DTNM, LMSE, F-38000 Grenoble, France

8 ^d Now at Aix Marseille Univ, CNRS, Centrale Marseille, ISM2, Marseille, France

9 ^{*}Corresponding author: e-mail: henri.wortham@univ-amu.fr Phone: (+33) (0)413551039

10 **ABSTRACT**

11 Given the toxic nature of many volatile organic compounds (VOCs) present within indoor settings,
12 it behooves the building engineering community to develop new control strategies for contaminant
13 removal to mitigate health impacts and improve well-being of human beings within building
14 environments.

15 Photocatalytic paints belong to a class of technologies potentially used to obtain self-cleaning wall
16 surfaces for air decontamination within building environments. They offer a promising solution
17 for the building engineering industry involved in paint manufacturing processes to produce paint
18 formulations that limit indoor air pollution and consequently individual exposition of inhabitants.
19 In this work, we report on the uptake efficiency of m-xylene on one reference paint and three

1 mineral paints impregnated with a photocatalytic agent, namely, a conventional photocatalyst
2 containing 3.5% of nano-TiO₂ and two new nano-TiO₂ photocatalysts coated with polyethylene
3 glycol (PEG 3350) and a hybrid cellulose nanocrystals-nano-TiO₂ (CNC) containing 3.5% and
4 0.5% of nanoparticles, respectively. The photocatalytic degradation of these paints under UV
5 irradiation and the consequent VOC emissions were assessed to evaluate the photocatalytic
6 stability of the nano-TiO₂ photocatalytic paints.

7 The experimental results obtained in this work did not show any photocatalytic activity and no
8 VOC emissions for the reference paint containing exclusively micro-TiO₂ (that is, no nano-TiO₂
9 material) particles under given experimental conditions. On the other hand, the obtained results
10 showed that the paint containing CNC nanoparticles (NPs) had only a finite photocatalytic effect
11 that was likely due to the low quantity of the nano-TiO₂ photocatalyst present within the paint
12 formulation matrix. Furthermore, it was observed that the paints containing nano-TiO₂ and
13 PEG 3350 NPs resulted in an important photocatalytic activity that, unfortunately, led to
14 consequential VOC emissions resulting from the polymeric matrix photo-oxidation reactivity
15 under the given experimental conditions employed. Overall, the experimental results obtained in
16 this work indicate that the paint containing PEG 3350 NPs had a greater photocatalytic activity
17 than the paint containing the nano-TiO₂ particles. Further, it was observed that the VOC emissions
18 of this PEG 3350 paint decreased with the aging time (28% and 10% for 500 hours and 1000 hours
19 of aging, respectively). Based on the experimental results obtained in this work, the new PEG
20 3350 photocatalyst is a more promising indoor pollutant decontamination engineering solution to
21 be used in mineral paint formulations to limit indoor air pollution.

22 **Keywords:** Indoor air, Uptake coefficient, VOC emissions, Photocatalytic paints, PTR-MS

23

1. INTRODUCTION

On average, humans spend over 90% of their lives indoors¹⁻³. Recent studies^{4,5} have shown that the breathed indoor air has indoor-to-outdoor environment VOC concentration ratios up to 14.3. This is worrisome since some of the VOCs commonly found within indoor environments are known to cause adverse human health effects. For example, some of the pollutants commonly found within indoor environments include known carcinogens such as benzene, dichloromethane, and formaldehyde⁶. Indoor VOC emission sources include household activities such as cooking and smoking, carpentry, household furnishing, and cleaning products, among others. Given the multitude of indoor emission sources of VOCs, the current focus of building authorities and construction industries has been to develop new technologies that include adsorption, biofiltration, condensation and/or photocatalytic oxidation (PCO) to improve indoor air quality and provide a saner indoor environment for its occupants⁷⁻⁹. As a result, a new generation of “cleaning” materials has been in development based on the PCO technique. The PCO technique takes advantage of the paints’ photocatalytic properties to oxidize and/or reduce air pollutants that adsorb on the semiconductor surfaces. This technique has been hailed as a promising new zero-emission technology that improves indoor air quality¹⁰ by destroying all the VOCs.

1 To better understand the essence of indoor air pollution, a series of model compounds known as
2 BTEX, namely, benzene, toluene, ethylbenzene and o-m-p xylenes, have been traditionally used
3 to study indoor air quality ¹¹⁻¹⁴. For example, Morin et al. (2020) has recently reported on the
4 photocatalytic degradation of gas-phase m-xylene on organic paints as a function of different
5 experimental conditions that included nano-TiO₂ content and nature, irradiance, relative humidity
6 (RH), surface temperature, pigment volume concentration (PVC) and aging in the lab ¹⁵. In their
7 work, Wortham and coworkers¹⁵ observed that the m-xylene degradation on organic photocatalytic
8 paints was strongly dependent on environmental parameters that included solar irradiance, %RH,
9 and surface temperature in addition to the paint composition, namely, the nano-TiO₂ content and
10 nature, PVC and aging. M-xylene has often been used to study photochemical degradation
11 processes within indoor settings because (1) it is observed in indoor air in trace amounts ¹⁶, (2) it
12 has well documented negative human health effects ¹⁴, (3) it is a relatively inert compound due to
13 its aromatic ring structure and (4) it is not used as a binder nor a solvent in paint preparation,
14 therefore, it is not emitted by studied paints ¹⁷, minimizing any unwanted experimental artifacts.

15 Even though the engineering motivation behind the development of photocatalytic paints has been
16 to solve the problem of indoor air pollution, many studies have reported contradictory or nuanced
17 results at best. That is, it is now well documented that photocatalytic paints do emit VOCs

1 themselves in the presence of UV radiation ^{4,17-20}. It has been proposed that under UV irradiation
2 the active radical species that include OH and O radicals generated on nano-TiO₂ surfaces react
3 with the binder molecules present within the paint matrix to produce and emit VOCs. The VOC
4 emission by photocatalytic paints under given environmental conditions has become a major
5 ‘green chemistry’ problem because all paint materials do contain organic solvents or organic
6 binders to a certain degree. However, the presence of organic binders in paints is structurally
7 important because it is the binder material itself that keeps the pigments in place after the paint
8 dries. Unfortunately, an important increase in emissions of different VOCs such as formaldehyde,
9 acetaldehyde, and acrolein under UV irradiation conditions has been observed for selected organic
10 photocatalytic paints ^{17,19,20}. Further, the photocatalytic reactions between the radical species and
11 binder molecules are important because they affect paint durability, have a negative impact on
12 indoor air quality, and limit the paint’s photocatalytic properties ²¹. The photo-degradation of the
13 binder may reduce the oxidative advantages of the PCO method as a ‘green-chemistry’ tool to
14 better indoor air.

15 One of the current engineering solutions to overcome this problem is to reduce the organic binder
16 content to 5% and to replace the remaining organic binder with a mineral one. Such mineral paints
17 have been studied under laboratory conditions by Morin et al. (2019). These investigators observed

1 a 43% decrease in total VOC emissions ¹⁷ when mineral paints were employed under given
2 experimental conditions, a very promising result. Considering these promising results, a new
3 generation of mineral photocatalytic paints have been developed to better indoor air quality.

4 In this laboratory work, the uptake coefficients of m-xylene and VOC surface emission fluxes for
5 mineral paints containing three different photocatalysts, namely, nano-TiO₂, PEG 3350 and CNC,
6 within the binder matrix were determined in the presence of UV radiation. The influence of aging
7 and the type of photocatalyst was evaluated using the comparative approach for uptake and
8 emissions. The obtained uptake and emission results were compared with the reference paints
9 uptake and emission results that did not contain any nano-TiO₂ photocatalyst material to determine
10 the impact of nano-TiO₂ on each photocatalytic paint. The obtained results will help to improve
11 future binder formulation materials to increase the paints' photocatalytic activities while
12 minimizing any corresponding VOC emissions from the photocatalytic paints. The obtained results
13 will help the building industry community to foster the development of paints and coatings that
14 will contribute to a better indoor quality for the occupants.

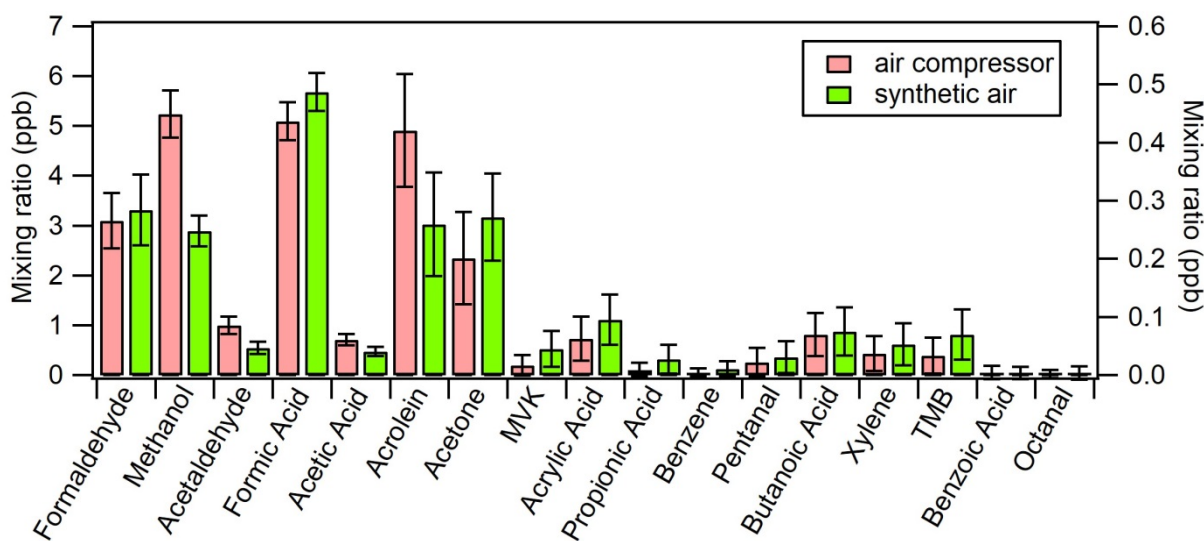
15 **2. MATERIALS AND METHODS**

2.1. Experimental study

The experimental approach used to study the uptake coefficient (γ) of m-xylene on photocatalytic and reference mineral paints is similar to the one used in a previous study on m-xylene photocatalytic degradation on selected organic paints¹⁵. The schematic representation of the experimental set-up and the experimental procedure have been published elsewhere^{15,17,19}. Only the experimental details that are particularly relevant to this work are given below.

Briefly, a borosilicate glass double-wall horizontal-flow-tube-reactor with an internal volume of about 131 cm³ was employed to study the uptake of m-xylene using the High-Sensitivity-Proton-Transfer-Reaction Mass Spectrometer (HS-PTR-MS) (IONICON Analytik, Austria) detection (see supporting information, Fig 1). The temperature within the reactor was maintained at a constant temperature, $T(K) = \pm 1$, by circulating deionized water through the outer jacket using a temperature-controlled circulating bath (RC6 LAUDA, Germany). The experiments were carried out at surface temperature values ranging from $T(K) = 292$ to 298. All experiments were carried out at $p = 1$ atm total pressure of air (SF2, Atlas Copco, Sweden) that was scrubbed using an activated carbon cartridge. The geometry of the flow-tube reactor was such that it allowed for the scrubbed air carrier gas flow to enter at one end and the HS-PTR-MS detection system to be located downstream at the opposite end.

1 The VOC impurity content of the scrubbed air carrier gas used in the m-xylene uptake experiments
 2 was compared with the VOC content of a certified synthetic air cylinder (Linde gas, France,
 3 >99.999% stated purity). The comparison of the VOC impurity content measured in the scrubbed
 4 air and in the Linde synthetic air cylinder is shown in Figure 1.



5
 6 Figure 1: VOC mixing ratios (ppb) obtained from air compressor (pink) and synthetic air bottle (green). Mixing ratios
 7 of formaldehyde to acetic acid are on the left axis and acrolein to octanal are on the right axis. Errors bars are $\pm 1\sigma$
 8 precision based on 70 experimental point values

9 As shown in Figure 1, most of the obtained mixing ratio values of the selected VOCs measured in
 10 the scrubbed air and in the synthetic air cylinder were well within their given uncertainty values.
 11 The only exception was the measured mixing ratio value of methanol. Here, the maximum
 12 methanol mixing ratio measured in the scrubbed air flow was 5.2 ppb, a value that was about twice
 13 the methanol mixing ratio value measured in the Linde gas cylinder. All the other measured mixing
 14 ratio values were observed to be < 1 ppb for the selected 14 VOCs, including m-xylene (0.04 ppb).

1 Further, additional emission experiments using the scrubbed air gas flow source and the Linde air
2 cylinder carrier gas flow source were carried out in the presence of photolyzing radiation. No
3 additional emission sources have been observed in the presence of the photolyzing light.

4 A typical experiment involved the m-xylene reactant that was allowed to enter the horizontal
5 reactor through a movable injector that permitted to vary the contact time between the m-xylene
6 and mineral paint surface to determine the uptake kinetics of the given heterogeneous reactions.

7 The selected paint was applied only on one side of the Leneta (black plastic-vinyl chloride/acetate
8 copolymer, Leneta company, U.S.A.) plate that was 26 cm long and 2 cm wide based on a standard
9 operating procedure developed by the manufacturer ALLIOS¹⁷. The plate covered by the selected
10 mineral paint was placed within the horizontal reactor with the painted side oriented up.

11 The reactor was placed within a stainless-steel box equipped with four UV fluorescent lamps
12 (Philips TL-D 18W Actinic BL, 340-400 nm, $\lambda_{\text{max}} = 368$ nm, length 60 cm) (see supporting
13 information, Fig 1). The four fluorescent lamps were placed side-by-side on the upper side of the
14 box and could be operated individually. The spectral irradiance of the lamps has been determined
15 previously by Wortham and coworkers (2014)²². The integrated UV spectral irradiance was
16 estimated to be 8.8 W m^{-2} and 18.6 W m^{-2} for 2 and 4 lamps, respectively, between $\lambda \sim 340$ nm to
17 400 nm. The experimental spectral irradiance was 8.8 W m^{-2} because this value represents an

1 averaged integrated irradiance from $\lambda \sim 340$ nm to 400 nm of solar light that is known to enter an
2 indoor environment (Bartolomei et al, 2014). The m-xylene uptake coefficient experiments carried
3 out at 18.6 W m^{-2} were performed to increase the MS detection sensitivity of the m-xylene signal
4 and to better determine the impact of the nano-TiO₂ photocatalyst.

5 Gas-phase m-xylene was generated using the gas-phase generator (PUL 200, Saint Chamas,
6 France) which consisted of a sealed Teflon permeation tube (Perfluoroalkoxy, 4.0 x 6.4 mm, 8 cm
7 long) filled with pure m-xylene (Sigma-Aldrich, $\geq 99.5\%$)¹⁵. The flow out of the generator was
8 10 sccm (Brooks SLA Series mass flow controller, in the range 0 to 10 sccm, $\pm 1\%$ stated accuracy)
9 and was allowed to enter the movable injector of the horizontal reactor. A sheath air flow of 190
10 sccm (Brooks SLA Series mass flow controller, in the range 0 to 500 sccm, $\pm 1\%$ stated accuracy)
11 was allowed to enter the reactor to dilute the m-xylene flow. The resulting experimental m-xylene
12 mixing ratio was ~ 40 ppb.

13 Relative humidity was adjusted by allowing a portion of the sheath airflow to enter a bubbler
14 containing deionized water (resistivity $> 18 \text{ M}\Omega \text{ cm}$). The %RH was measured continuously using
15 the “Hygrolog NT2” (Rotronic) hygrometer with “HygroClip SC04” probe located at the exit of
16 the reactor. The experiments were carried out at relative humidity values that ranged from 1% to
17 42% and the experimental uncertainty in the relative humidity value measurements was $\pm 1.5\%$ RH.

1 The m-xylene mixing ratio was measured online using the HS-PTR-MS by following its mother
 2 ion pic m/z 107. Similar to our previous work on VOC emissions on selected organic photocatalytic
 3 paints, 16 other signature VOC model compounds were measured continuously and online using
 4 the HS-PTR-MS analyzer ¹⁷. The list of all the VOCs identified using the HS-PTR-MS system
 5 including the corresponding mass-to-charge (m/z) ratios of the corresponding mother ions are
 6 given in Table 1¹⁷.

7 Table 1. Compounds detected and quantified using the HS-PTR-MS technique.

Compounds	m/z	References
Formaldehyde	31	23 ; 24
Methanol	33	25 ; 24 ; 26
Acetaldehyde	45	23 ; 25 ; 24 ; 26
Formic Acid	47	24
Acrolein	57	24
Acetone + Propanal	59	23 ; 25 ; 24 ; 26
Acetic Acid	61	25 ; 24 ; 27 ; 26
Methyl Vinyl Ketone	71	25 ; 24
Acrylic Acid	73	19
Propionic Acid	75	27
Benzene	79	23 ; 25 ; 24 ; 26
Pentanal + Vinyl Acetate	87	23 ; 19
Butanoic Acid	89	27
Ethylbenzene + Xylene	107	23 ; 25 ; 24
Trimethylbenzene + Ethyltoluene	121	23 ; 25 ; 24
Benzoic Acid	123	26 ; 19
Octanal	111 & 129	19

8
 9 The compounds listed in Table 1 have been chosen as model compounds by the scientific
 10 community to represent major chemical families typically observed within indoor air settings,
 11 namely, family of acids, carbonyl compounds, aromatics, and alcohols.

1 Similar to our previous work on organic paints, the HS-PTR-MS analyzer drift pressure and drift-
2 tube temperature were fixed at $p(\text{mbar}) = (2.23 \pm 0.01)$, $T(\text{K}) = (333 \pm 1)$, respectively ¹⁷. The drift
3 tube voltage was 500 V. This value corresponded to the electric field (E , V cm^{-1}) to ambient air
4 number density (N , cm^{-3}) ratio (E/N) value of 124 Townsend (1 Townsend = 10^{-17} V cm^2).

5 **2.2. Preparation of paints**

6 Mineral paints were formulated and produced by a local paint manufacturer ALLIOS (Marseille,
7 France). Three types of nanoparticles used to formulate the selected paints included (1) nano-TiO₂
8 PC500 in anatase form, (2) nano-TiO₂ coated by bio-inspired ligand polyethylene glycol (PEG
9 3350) and (3) nano-TiO₂ grafted onto cellulose nanocrystals (CNC). The synthesis of the new
10 types of photocatalytic TiO₂ NPs as well as their characterization has been published in detail by
11 Rosset and coworkers (2021) (Rosset et al., 2021).

12 These newly synthesized TiO₂ NPs were physically incorporated into the mineral matrix-based
13 paint by the manufacturer ALLIOS (France) using a standard operating procedure used in paint
14 industry. First, a mixture of ground additives (slurry) was prepared with each of the active
15 nanosized TiO₂ form listed above. Then, the paint of mineral matrix-based was mixed with the
16 slurry to reach the desired quantity of nano-TiO₂ within the paint matrix. The nano-TiO₂ percent
17 weight obtained in the slurry, paint, and finally in the dry paint are presented in Table 2. The

1 obtained slurry nano-TiO₂ percent composition, slurry in paint and the paint nano-TiO₂ percent
2 compositions are presented in Table 2. Mineral binders contained 5% of the organic binder to help
3 the drying process of the paint on the Leneta surface so that only non-volatile content of paint
4 remained after the coating solidified. We underline that no nano-TiO₂ particle content was present
5 in the reference paint.

6 **Table 2: Percent compositions of nanoparticles in slurry (%), paint (%) and dry paint (%) used in this work.**

Paint	Nano-TiO ₂ in slurry (%) (w/w)	Slurry in paint (%) (w/w)	Nano-TiO ₂ final dry content (%) (w/w)
Reference	0	0	0
nano-TiO ₂	35	10	3.5
PEG 3350	35	10	3.5
CNC	13.7	3.65	0.5

7
8 The paints were applied only on one side of Leneta supports according to a standard operating
9 procedure developed by the manufacturer ALLIOS²⁸. This procedure allowed for production of
10 homogeneous, uniform and reproducible wet films that were 100 μm thick. Then, the paints were
11 stored for 21 days at T(K) = 296 while a humidified (55%RH) synthetic air was allowed to flow
12 over the plates. The resulting paint thickness was 40 μm. To assure proper fit into the reactor, the
13 Leneta support was fixed on a glass plate with wire to both ends prior to experiments.
14 Reference and the three photocatalytic paints have been aged in an accelerated aging chamber
15 (model QUV accelerated weathering, Q-Lab, U.S.A.) for 500 hours and 1000 hours according to

1 the ISO norm 16474-3^{29,30}. Aging time of 500 hours corresponded to a well-aged paint and the
2 aging time of 1000 hours corresponded to a paint at the end of its lifetime.

3 Before and after the process of artificial paint weathering, the paints' surface morphology was
4 investigated using the scanning electron microscopy (SEM-FEG, LEO 1530, Germany). In
5 addition, the surrounding environment of elements present at the near paint surfaces (first 10 μm)
6 were investigated using the X-ray photoelectron spectroscopy (XPS, Versaprobe II ULVAC-PHI
7 spectrometer, Japan). The experimental protocol and the characterization results have been
8 published in detail by Boutry *et al.*, (2017) and Rosset *et al.*, (2021).

9 **2.3. Kinetic measurements**

10 One on the aims of this study was to evaluate the uptake coefficient (γ) values of m-xylene on
11 photocatalytic and reference mineral paints. The uptake coefficients were calculated using

12 Equation 1³¹:

$$13 \quad \gamma = \frac{4k_{1st}}{\omega} \frac{V}{S} \quad \text{Eq. 1}$$

14 where ω is the mean molecular velocity (cm s^{-1}), V/S is the ratio of the volume of the reactor to
15 surface area of the Lenata plate (cm) and k_{1st} the pseudo-first order rate constant of m-xylene loss
16 (s^{-1}).

1 The rate constant (k_{1st}) was calculated using the linear regression of the slope of $\ln(C_0/C_x)$ plotted
 2 as a function of the residence time (t) ^{15,22,32}. The C_0 was the m-xylene initial concentration at the
 3 position P_0 , that is, when the injector was all the way in the horizontal flow reactor and the m-
 4 xylene was not allowed to encounter the mineral paint surface. The C_x was the m-xylene
 5 concentration at different positions of the injector that ranged from P_1 to P_4 (Table 3). More
 6 precisely, the P_1 to P_4 injector positions refer to different distances of the injector as it was moved
 7 back within the horizontal flow-tube reactor.

8 Table 3. Distance to the end of reactor (cm), residence time (s) and exposed surface (cm²) between gaseous m-xylene
 9 and mineral paint as a function of movable injector position.

Injector position	Distance (cm)	Exposed surface (cm ²)	Residence time (s)
P_0	0	0	0
P_1	4	8	5.4
P_2	8	16	10.9
P_3	15	30	20.4
P_4	22	44	29.9

10

11 The difference between C_0 and C_x corresponds to the amount of m-xylene consumed by different
 12 physical and reactive processes that occur on the mineral paint surface that include loss by reaction,
 13 dry deposition, adsorption, and reactive loss by reaction with impurities, albeit, considered to be
 14 negligible. In a typical experiment, each injector position was held for at least 30 minutes to
 15 stabilize the signal and to reduce the impact of signal fluctuation and variability and to minimize

1 the effects of noise factors. After each P_x ; the movable injector was pushed in to its original P_0
2 position to obtain, again, the C_0 value.

3 Blank experiments were carried out to ensure that no other reactive or physical wall loss processes
4 occurred during the experiments. Further, the Cooney-Kay-Davis method was used to correct the
5 obtained uptake coefficient values from diffusion limitation in the flow tube^{33,34}.

6 **2.4. VOCs mixing ratio and estimation of surface emission fluxes**

7 Based on the original work of Lindinger and coworkers^{35,36} and our previous work on
8 photocatalytic paint emissions^{15,17}, the mixing ratio (ppb) was calculated using the Equation 2.

$$9 \quad C_x = 1.65 \times 10^{-11} \times \frac{U_{drift} \times T_{drift}^2}{k \times P_{drift}^2} \times \frac{i[X]}{i[H_3O^+] + Xr \times i[H_3O^+(H_2O)]} \quad \text{Eq. 2}$$

10 where U_{drift} is the drift tube voltage (V), T_{drift} is the drift tube temperature (K), k is the proton-
11 proton-transfer reaction constant ($\text{molecule cm}^3 \text{ s}^{-1}$), P_{drift} is the pressure within the drift-tube
12 (mbar), $i[X]$, $i[H_3O^+]$ and $[H_3O^+(H_2O)]$ are the ion signal counts per second of the target compound
13 (X), hydronium ion (H_3O^+) and hydronium ion cluster ($H_3O^+(H_2O)$), respectively, normalized by
14 the corresponding transmission efficiency.

15 The m/z specific relative transmission efficiency was experimentally determined over the mass
16 range of 21-181 with a calibration gas standard, consisting of a mixture of 14 aromatic organic

1 compounds (TO-14A Aromatic Mix, Restek Corporation, Bellefonte, USA, 100±10 ppb in
2 Nitrogen).

3 The factor X_r is compound specific and has been described in detail by de Gouw et al. ²⁵ and
4 reflects both the difference in the rate coefficient for the proton-transfer-reactions $H_3O^+ + R$ and
5 $H_3O(H_2O)^+ + R$ and the difference in transmission efficiencies for the two reagent ions within the
6 quadrupole mass filter region of the mass spectrometer. Different values for k and X_r used in this
7 work have been taken from our previous work on VOC emissions from indoor photocatalytic
8 paints ¹⁷.

9 The surface emission fluxes (molecule $cm^{-2} s^{-1}$) were determined using the following Equation 3.

10 Surface Emission Fluxes $X = \frac{C_x \times 2.46 \times 10^{10} \times \text{Internal reactor volume}}{(\text{Residence time} \times \text{Exposed paint surface})}$ Eq. 3

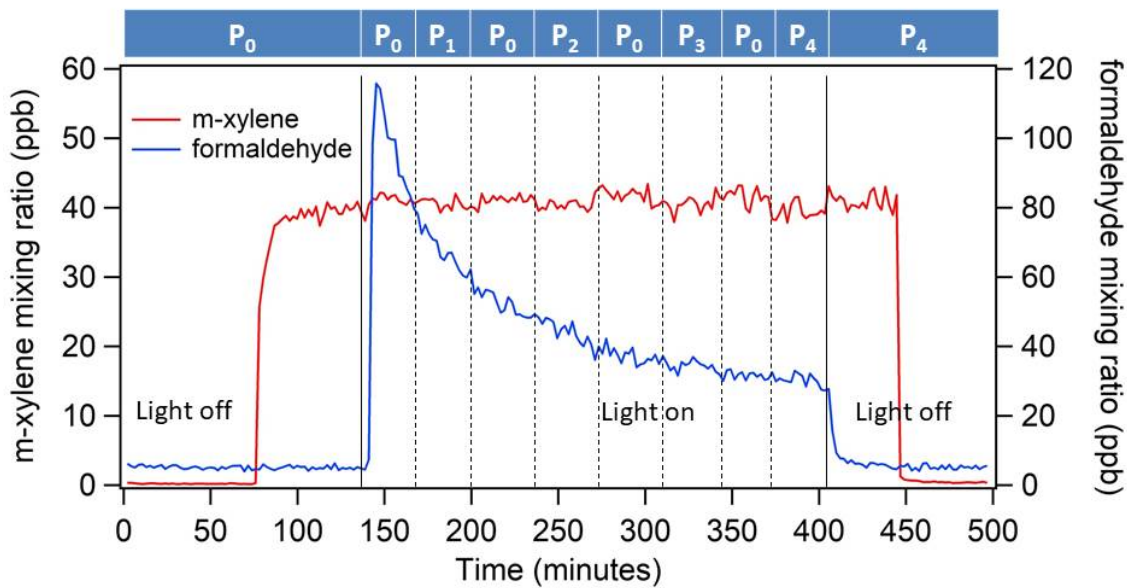
11 where the internal reactor volume, the residence time within the reactor and the exposed paint
12 surface area are expressed in units of cm^3 , s and cm^2 , respectively, The C_x is the mixing ratio (ppb)
13 measured at the exit of the reactor as a function of time for the target compounds. The 2.46×10^{10}
14 value is the ppb to molecule $cm^{-3} s^{-1}$ conversion factor calculated using the ideal gas law under
15 normal pressure and standard temperature conditions.

16 3. RESULTS AND DISCUSSION

1 In a typical investigation of the uptake coefficient of m-xylene on a given photocatalytic mineral
2 paint, the Leneta support with a painted surface up was first placed within the horizontal reactor
3 and the injector was pushed through completely (position P_0) so that no contact was allowed
4 between the m-xylene flow and the painted surface. The studied paint was then allowed to rest
5 within the horizontal flow reactor under “dark” conditions, that is, with the UV lamps off, for 2
6 hours under given experimental conditions of temperature and flow dynamics. At this time, since
7 the photocatalytic properties of the paint were not activated in the absence of UV irradiation, the
8 “dark” VOC emissions were determined. Furthermore, during this time, since m-xylene was
9 allowed to flow into the reactor without any contact with the painted surface, the m-xylene initial
10 mixing ratio value, C_0 , was measured. After a given time, the UV lights were turned on. Here, in
11 the presence of UV irradiation, the photocatalytic properties of the paint were activated and the
12 photocatalytically formed reactive species, namely hydroxyl radicals ($\cdot\text{OH}$), superoxide radicals
13 ($\cdot\text{O}_2^-$) and hydrogen peroxide radicals ($\cdot\text{OOH}$)³⁷, reacted with m-xylene and binder organic
14 constituents present on the surface of the TiO_2 catalyst^{21,30}.

15 As shown in Figure 2, upon exposure of the painted surface to UV irradiation, a formation of
16 formaldehyde was observed. More precisely, an intense response to the gas-phase formaldehyde
17 ion by the mass analyzer was observed as soon as the UV lamps were turned on. The formation of

1 gas-phase formaldehyde was observed independent of the injector position with respect to the
2 exposed (or not) painted surface within the horizontal flow-tube reactor. For example, the initial
3 injector position, P_0 , with the UV lamps on allowed to check if there was any photo-degradation
4 of m-xylene within the movable injector itself. After, the m-xylene mixing ratio, C_x , was measured
5 on-line at a given injector position, P_x , over the painted surface within the horizontal flow-tube.
6 Finally, when the injector was all the way “out” and the entire painted surface within the reactor
7 was exposed to the m-xylene flow (position P_4), the UV lights were turned off and the selected
8 VOC emissions were monitored continuously for 2 hours. Here, the comparison of the m-xylene
9 mixing ratio in position P_4 while the UV lamps were on and P_4 while the UV lamps were off was
10 used to verify if the m-xylene degradation in position P_4 was due to photocatalytic destruction or
11 other chemical or physical phenomena.



1

2 Figure 2: Typical temporal profile of m-xylene (red line) and formaldehyde (blue line) mixing ratio at 298 K, RH =
 3 40%, irradiance 8.8 W m⁻², aging: 500 hours and nano-TiO₂ PEG 3350. Px corresponds to the different position of the
 4 movable injector during the experiment.

5 As may be seen in Figure 2, the typical m-xylene temporal profile obtained for mineral
 6 photocatalytic paint PEG 3350 was contrary to the expected results where the gas-phase m-xylene
 7 was expected to degrade once in contact with the painted surface. In fact, no degradation of m-
 8 xylene was observed as the injector position was varied, thus, allowing the m-xylene to come in
 9 contact with the painted surface. Such an expected decrease in the m-xylene mixing ratio was
 10 observed in our previous study on photocatalytic destruction of selected VOCs on organic
 11 photocatalytic paints¹⁵. To our great surprise and contrary to our previous work on reactivity of
 12 organic photocatalytic paints, the photocatalytic activity of mineral photocatalytic paints seemed
 13 to be non-existent or negligible at best.

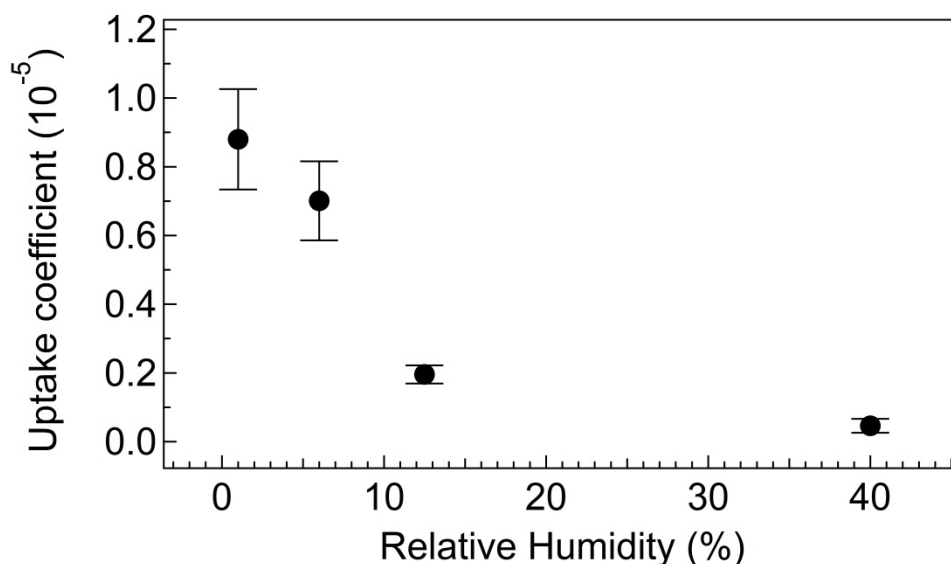
1 As shown in Figure 2, contrary to the m-xylene signal profile, the measured formaldehyde
2 temporal profile was observed to differ. In fact, when the UV lights were turned on, the
3 formaldehyde mixing ratio signal was observed to increase significantly. On the other hand, once
4 the UV lamps were switched off, the formaldehyde mixing ratio was observed to decrease
5 immediately to reach its initial value within few minutes. This important impact of irradiance
6 showed the presence of photocatalytic activity in the binder. Further, the observed emissions of
7 low molecular carbonyl compounds such as formaldehyde is consistent with other studies on UV
8 irradiation of photocatalytic paints ^{38,39}.

9 Based on the m-xylene and formaldehyde temporal profile results described above, it may be
10 concluded that the PEG 3350 mineral paint was photocatalytically active. However, the m-xylene
11 was unable to reach the radical species on the photocatalytic paint surface to react. We propose
12 several reasons for the observed phenomenon. One of the reasons is that the water vapor competed
13 with the gas-phase m-xylene for adsorption on the active site of the photocatalyst ⁴⁰⁻⁴². Another
14 possibility is that a thin layer of water formed on the painted surface, thus, hindering the interaction
15 between the gas-phase m-xylene and the radical species ⁴³. The formation of this thin layer of
16 water on nano-TiO₂ is facilitated because mineral binder is more porous and more permeable to
17 water vapor ⁴⁴ than the organic binder. Additional experiments were performed to better

1 understand the observed lack of photocatalytic destruction of m-xylene on selected mineral paints
2 under the experimental conditions employed.

3 **3.1. RH impact**

4 Investigations into the relationship between the photocatalytic activity of TiO₂ organic binder
5 paints and relative humidity has already been investigated by Martinez et al. and Wortham and
6 coworkers^{15,45}. These investigators have reported that the photocatalytic activity of selected TiO₂
7 organic binder paints decreased by a factor of two when relative humidity was increased. Similar
8 to the investigations into the relationship between the photocatalytic activity of TiO₂ organic
9 binder paints and relative humidity cited above, m-xylene uptake rate experiments were performed
10 on TiO₂ mineral binder paints used in this work as a function of relative humidity. The effect of
11 the RH on measured uptake coefficient values of m-xylene on selected TiO₂ mineral binder paint
12 is shown in Figure 3.



1

2 Figure 3: The observed effect of relative humidity on the measured uptake coefficient of m-xylene on selected TiO₂
 3 mineral binder paints. Experimental conditions: Active ingredient = nano-TiO₂ PEG 3350, [m-xylene] = 40 ppb,
 4 T = 292 K, light intensity = 18.6 W m⁻², aging = 500 hours. Error bars are derived from uncertainties associated to
 5 uptake coefficient.

6 As shown in Figure 3, an increase in relative humidity was observed to lead to a decrease in the

7 measured uptake coefficient values of m-xylene on selected TiO₂ mineral paints. For example, the

8 uptake coefficient of m-xylene was calculated to be $\gamma = (8.8 \pm 1.5) \times 10^{-6}$ at 1% RH and $\gamma =$

9 $(4.6 \pm 2.0) \times 10^{-7}$ at 40% RH. The observed almost two orders of magnitude decrease in the

10 measured uptake coefficient value with increasing relative humidity may have been a result of

11 physical competition for access to the radical species present on the paint's nano-TiO₂ surface

12 between the water molecules and m-xylene. More precisely, at low humidity, m-xylene may not

13 have had to compete for access to the active surface sites of the photocatalytic paint, resulting in a

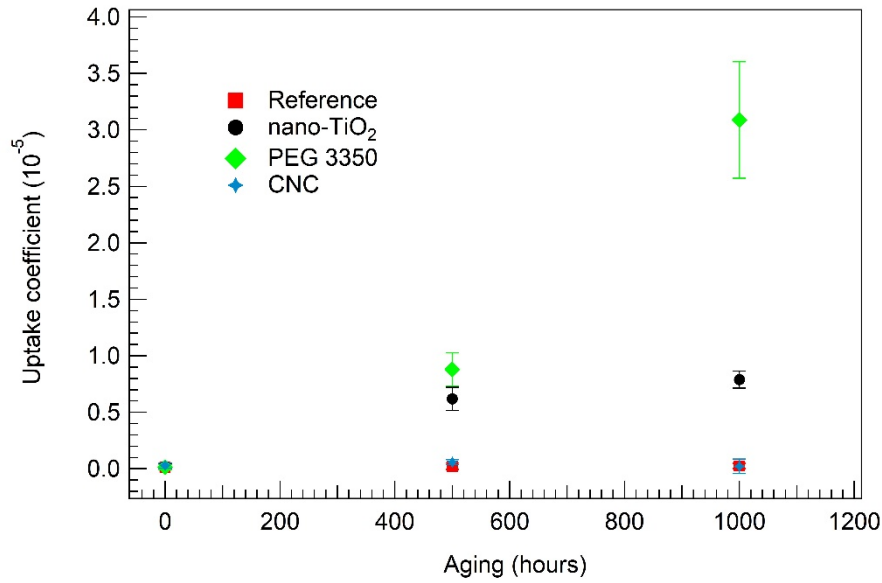
14 more effective degradation of m-xylene; an argument that is supported by a higher uptake

15 coefficient value. On the other hand, as the experimental RH was allowed to increase, the

1 competition between the water molecules and the gas-phase m-xylene to access the active sites of
2 the photocatalytic paint surface likely resulted in a decrease in the overall photocatalytic
3 heterogeneous reactivity of the paint ⁸; a result that is supported by lower m-xylene uptake
4 coefficient values in the presence of water vapor. In view of the obtained relative humidity effect
5 results and to better compare the m-xylene uptake on selected paints, experiments were carried
6 using low relative humidity values within the horizontal flow-tube reactor.

7 **3.2. Uptake coefficients**

8 To better characterize the photocatalytic properties of paints, m-xylene uptake coefficients were
9 measured on weathered paint supports. Here, the selected paints were exposed to fluorescent UV
10 lamp radiation, heat and water under controlled laboratory conditions to reproduce the aging
11 effects that occur under real-environment conditions ^{29,30}. The effects of paint aging on the
12 measured m-xylene uptake coefficients are shown in Figure 4. The aged paints included a reference
13 paint and three photocatalytic paints. The reference paint did not contain any nano-TiO₂ content
14 and only micro-TiO₂ pigments used in paint formulations. On the other hand, in addition to the
15 micro-TiO₂ pigment content present in all paints, the nano-TiO₂ and PEG 3350 photocatalytic
16 paints contained 3.5% of the nano-TiO₂ content and the CNC photocatalytic paint contained 0.5%
17 of the nano-TiO₂ content.



1

2 Figure 4: The effect of aging and photocatalyst on uptake coefficient of m-xylene. m-xylene mixing ratio: 40 ppb,
 3 temperature: 292 K, light intensity: 18.6 W m⁻², RH: 1%, reference paint (red square), paint nano-TiO₂ (black circle),
 4 paint PEG 3350 (green lozenge), paint CNC (blue lozenge). Error bars are derived from uncertainties associates to
 5 uptake coefficient.

6 As shown on the Figure 4, prior to aging, reference and photocatalytic paints m-xylene uptake

7 coefficient values were calculated to be in the range $\gamma = (1.4 \pm 2.1 - 2.8 \pm 2.3) \times 10^{-7}$. These

8 low uptake coefficient values may be explained by limited or finite binder degradation in the

9 absence of aging conditions that may physically circumscribe the contact between the radical

10 species produced by the nano-TiO₂ particles and m-xylene reactant gas. On the other hand, as

11 shown in Figure 4, once the paints have begun to weather under UV radiation, the m-xylene uptake

12 coefficient values have been observed to increase resulting in the upper-limit values of $\gamma = (7.9 \pm$

13 $0.7) \times 10^{-6}$ and $\gamma = (3.1 \pm 0.5) \times 10^{-5}$ for nano-TiO₂ and PEG 3350 paints, respectively. The

14 effect of aging on the paint's binder material has been previously observed and reported by Rosset

15 et al. (2021), Wortham and coworkers (2020) and Truffier-Boutry et al. (2017)^{15,21,30}. These

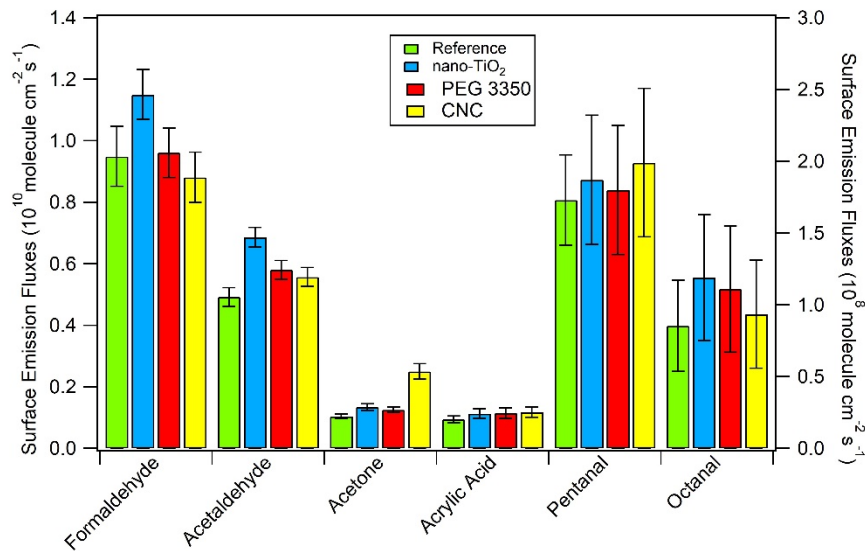
1 investigators reported that with aging, as paints were exposed to aging conditions that degraded
2 paint' binder material, nano-TiO₂ particles became physically more accessible to react with gas-
3 phase m-xylene, hence, increasing the paints' photocatalytic activities. That is, as the paint binder
4 content was observed to degrade with "age" under taxing environment conditions, the uptake
5 coefficient values were observed to increase. For example, while the nano-TiO₂ paints were
6 manufactured using nano-TiO₂, PEG 3350 paints were fabricated using the nano-TiO₂ coated with
7 bio-inspired ligand polyethylene glycol. The presence of the bio-inspired ligand polyethylene
8 glycol coating likely modified the physical and chemical characteristics of the nano-TiO₂
9 compared to the nano-TiO₂ paint formulation that lacked such a coating. This conjecture is
10 supported by a recent work carried out by Laisney et al. (2021) on the spatial repartition of
11 nanoparticles within the binder matrix, particle size and the nano-TiO₂ aggregation-to-
12 agglomeration ratio ⁴⁶. On the other hand, the nano-TiO₂ present in the PEG 3350 paints were
13 more dispersed within the binder, the particle size was bigger, and the aggregation-to-
14 agglomeration ratio was lower compared to the nano-TiO₂ paints. This modification allowed to
15 increase the quantity of active sites present on the paint surface resulting in an increased
16 photocatalytic activity.

1 As may be seen in Figure 4, the measured uptake coefficient values were observed to be
2 independent of the aging process and no photocatalytic activity has been observed for reference
3 and CNC paints. As shown in Figure 4, the presence of micro-sized TiO₂ particles within the
4 reference paint's formulation did not have any observable effect on its photocatalytic properties.
5 Further, the absence of photocatalytic activity in the CNC paints may be explained (1) by the
6 hybrid CNC-nano-TiO₂ protective properties of the binder staving off the photocatalytic
7 degradation of m-xylene and (2) the low quantity of nano-TiO₂ particles present within the CNC
8 paint matrix to allow any observable m-xylene degradation. To better examine these two
9 hypotheses, an increase of the nano-TiO₂ content of the CNC paint binder may be imagined.
10 Unfortunately, at this point such higher nano-TiO₂ formulation of CNC paints is not industrially
11 possible.

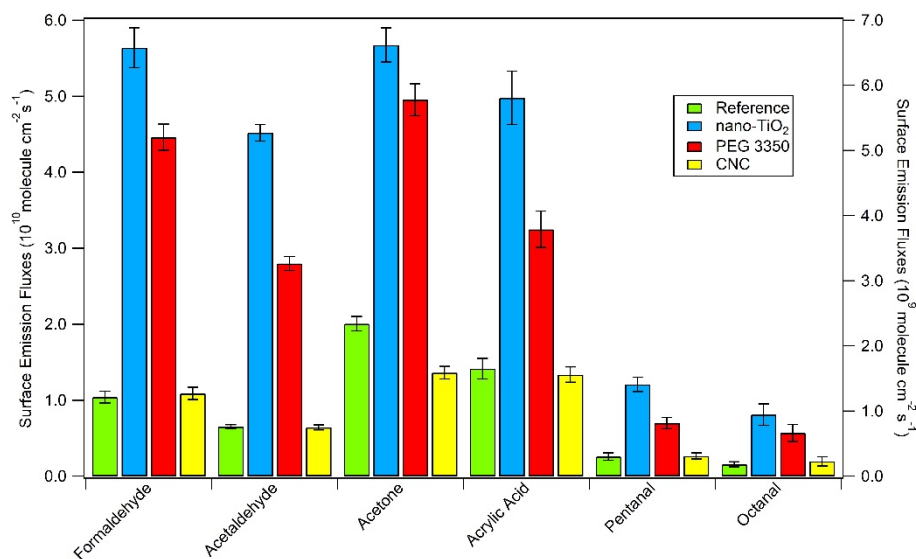
12 **3.3. VOC emissions**

13 VOC emissions from reference and three photocatalytic paints have been studied as a function of
14 weathering laboratory conditions that mirror a real environment. As may be seen in the supporting
15 information Table S1-S4, no emissions due to a photocatalytic activity have been observed for
16 methanol, formic acid, acrolein, acetic acid, MVK, propionic acid, benzene, butanoic acid, TMB
17 and benzoic acid. VOC-emission results obtained for other compounds for the selected paints that

1 have not been weathered are in Figure 5, at $t = 500$ hours and $t = 1000$ hours of aging time are
2 shown in Figure 6 and Figure 7, respectively.



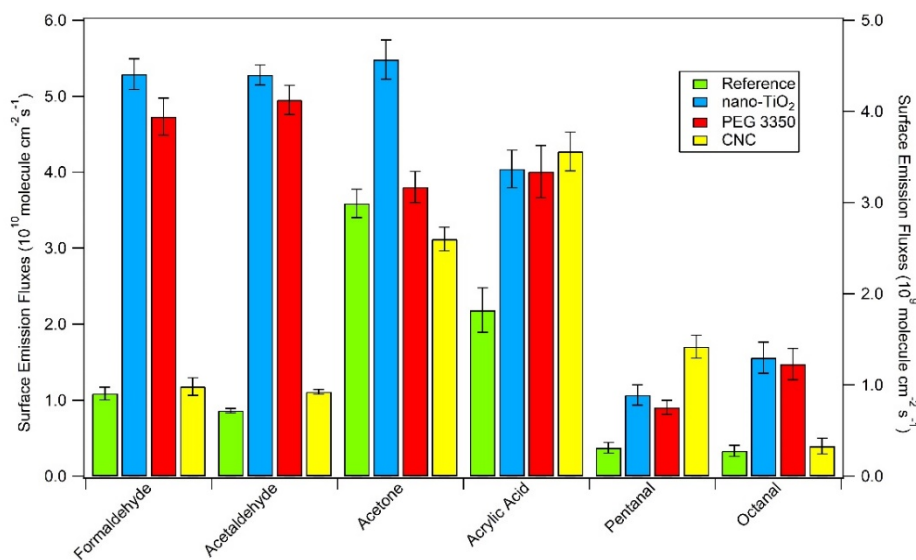
3
4 Figure 5: VOCs surface emission fluxes ($\text{cm}^{-2} \text{s}^{-1}$) obtained for selected compounds under UV irradiation. Surface
5 emission fluxes for formaldehyde, acetaldehyde, acetone and acrylic acid on the left axis and pentanal and octanal on
6 the right axis. Experimental conditions: $T = 298 \text{ K}$, 40% RH, solar irradiance = 8.8 W m^{-2} , aging = 0 hours. Error bars
7 are 1σ precision based on twenty experimental data point values.
8 As may be seen in Figure 5, the VOC surface emission flux values for reference and photocatalytic
9 paints were observed to be equivalent for all listed compounds. As a result, it was assumed that
10 any reactive interactions between the organic compounds present within the binder and the nano-
11 TiO_2 particles did not take place that would prevent or limit VOC emissions.



1

2 Figure 6: VOCs surface emission fluxes (molecule cm⁻² s⁻¹) obtained for selected compounds under UV irradiation.
 3 Surface emission fluxes for formaldehyde and acetaldehyde on the left axis and acetone, acrylic acid, pentanal and
 4 octanal on the right axis. Temperature: 298 K, RH: 40%, Irradiance: 8.8 W.m⁻², aging 500 hours. Error bars are 1σ
 5 precision based on twenty experimental point values.

6



7

8 Figure 7: VOCs surface emission fluxes (molecule cm⁻² s⁻¹) obtained for selected compounds under UV irradiation.
 9 Surface emission fluxes for formaldehyde and acetaldehyde on the left axis and acetone, acrylic acid, pentanal and
 10 octanal on the right axis. Temperature: 298 K, 40% RH, solar irradiance: 8.8 W.m⁻², aging 1000 hours. Error bars are
 11 1σ precision based on twenty experimental point values.

1 For reference paints, VOC emissions were observed to be independent of the aging process for
2 most of the listed compounds. However, as may be seen in Table S1, an increase of 75% in
3 acetaldehyde emission has been observed between 0 and 1000 hours of aging. The observed
4 increase in acetaldehyde emission may be due to a low quantity of the photocatalyst present within
5 the paint's binder ²¹. Overall, VOC photocatalytic emissions values were observed to be very low.
6 This observation demonstrates that micro-TiO₂ pigments have a negligible effect on the paint's
7 photocatalytic properties.

8 As shown in Table S4, an increase in VOC emissions has been observed at t = 1000 hours of aging
9 time for CNC paints. An increase of 34% in formaldehyde emissions, 99% in acetaldehyde
10 emissions, 204% in pentanal emissions and 253% in octanal emissions have been observed at 1000
11 hours of aging time compared to paints that have not been weathered. The observed increases in
12 VOC emissions are likely the result of a presence of 0.5% of nano-TiO₂ within the paint's binder.

13 At t = 1000 hours of aging time, the binder is likely degraded to result in an enhanced interaction
14 between the paint's organic fraction present within the binder and the nano-TiO₂ particles. As
15 shown in Figure 6 and Figure 7, The CNC paint VOC emissions are observed to be negligible
16 compared to an increase in VOC emissions observed for nano-TiO₂ and PEG 3350 paints.

1 Shown in the supporting information, nano-TiO₂ (Table S2) and PEG 3350 paint (Table S3) VOC
2 emissions are observed to increase significantly between t = 0 hour and t = 500 hours of aging time
3 and become constant between t=500 hours and t=1000 hours of aging time apart from acetaldehyde
4 and octanal emissions which are observed to increase. The observed difference in VOC emissions
5 between the photocatalytic paints and the reference paint demonstrates that the paint VOC
6 emissions are due to a photocatalytic effect resulting from a presence of nano-TiO₂ content. For
7 example, an observed increase in acetaldehyde emissions of a factor 5.4 and 4.3 has been observed
8 at t = 1000 hours of aging time for paints photocatalytic paints nano-TiO₂ and PEG 3350,
9 respectively, compared to the reference paint (Figure 7).

10 The VOC emissions are observed to be lower for PEG 3350 paints compared to nano-TiO₂ after
11 t = 500 hours and 1000 hours of aging time. A decrease of 21%, 34% and 13% of VOC emissions
12 has been observed for formaldehyde, acetaldehyde, and acetone, respectively, for PEG 3350 paints
13 compared to nano-TiO₂ paints at t=500 hours of aging time (Figure 6). A decrease of 11%, 7%
14 and 31% for formaldehyde, acetaldehyde, and acetone emissions, respectively, has been observed
15 for PEG 3350 paints compared to nano-TiO₂ paints at t=1000 hours of aging time (Figure 7). That
16 is, the PEG 3350 paints are observed to emit less VOCs than nano-TiO₂ paints. All surface
17 emission fluxes are listed in Table S1-S4 in Supporting Information.

4. CONCLUSION

Uptake coefficients and VOC emissions have been measured for one reference mineral paint containing three different kinds of TiO₂ nanoparticles, namely, nano-TiO₂, PEG 3350 and CNC. Their performances were compared to the same industrial paint containing no nanoTiO₂ whatever its form. The obtained laboratory results contribute to improve the understanding and knowledge on the impact of nano-TiO₂ photocatalysts present within paints on VOC loss and emissions within indoor environments. The obtained results are important to better indoor air quality and/or limit indoor VOC sources that may induce adverse effects on human health or well-being.

The laboratory results obtained in this work showed that the reference paint's micro-TiO₂ pigment content did not result in m-xylene degradation and VOC emissions were measured to be negligible, a result that is in agreement with our previous work on micro-TiO₂ pigment organic paints^{15,30}.

The absence of photocatalytic activity of the new CNC photocatalytic mineral paints may be explained by different binder effects such as (1) the hybrid CNC-nano-TiO₂ protective role of the binder staving off the photocatalytic degradation of m-xylene and (2) the 0.5% nano-TiO₂ content may be too low to allow any m-xylene uptake or loss.

While the m-xylene uptake coefficient experiments carried out using nano-TiO₂ and PEG 3350 paints resulted in an interesting photocatalytic activity, these paints were shown to emit VOCs.

1 Globally, the photocatalytic activity was observed to be more important for the newer PEG 3350
2 photocatalytic paint than the older nano-TiO₂ photocatalyst. Further, the newer PEG 3350
3 photocatalytic paint was observed to result in less VOC emissions compared to the older nano-
4 TiO₂ photocatalytic paint. Clearly, more studies and engineering work is warranted to improve
5 future paint formulations using the PEG 3350 photocatalyst content to better indoor air
6 environment.

7 The mineral photocatalytic paints are a promising, albeit challenging, innovation for the building
8 industry involved in paint manufacturing processes to produce “cleaner” paint formulations that
9 limit indoor air pollution and better indoor air environment. A photocatalytic activity of mineral
10 paints and the VOC emissions of mineral photocatalytic paints are observed to be lower than that
11 of photocatalytic organic paints. However, to better quantify the photocatalytic effects in addition
12 to environmental benefits and disadvantages, of mineral and organic paints, experiments need to
13 be carried out under real-environment conditions.

14 **ACKNOWLEDGMENTS**

15 The authors thank and acknowledge Isabelle Michaud-Soret (CEA, Grenoble) for the synthesis of
16 PEG 3350 nanoparticles, Isabelle Capron (INRA, Nantes) for the synthesis of CNC nanoparticles.
17 The authors acknowledge gratefully LABEX SERENADE (no.ANR-11-LABX-0064) funded by

1 the French National Research Agency (ANR) through the PIA (Programme Investissement
2 d'Avenir).

3 **ASSOCIATED CONTENT**

4 **Supporting Information**

5 Reference paint surface emission fluxes (Table S1), nano-TiO₂ paint surface emission fluxes
6 (Table S2), PEG 3350 paint surface emission fluxes (Table S3) and CNC paint surface emission
7 fluxes (Table S4), schematic presentation of the horizontal flow-tube reactor (Fig 1).

8 **Notes**

9 The authors declare no competing financial interest.

10

1 1 W. C. Roberts, J., Nelson, U. S. *Environ. Prot. Agency USEPA*.

2 2 N. E. Klepeis, W. C. Nelson, W. R. Ott, J. P. Robinson, A. M. Tsang, P. Switzer, J. V. Behar, S. C. Hern
3 and W. H. Engelmann, *J. Expo. Sci. Environ. Epidemiol.*, 2001, 11, 231–252.

4 3 J. Robinson and W. C. Nelson, *USEPA Res. Triangle Park NC*.

5 4 O. Geiss, G. Giannopoulos, S. Tirendi, J. Barrero-Moreno, B. R. Larsen and D. Kotzias, *Atmos. Environ.*,
6 2011, 45, 3676–3684.

7 5 M. Verrièle, C. Schoemaeker, B. Hanoune, N. Leclerc, S. Germain, V. Gaudion and N. Locoge, *Indoor*
8 *Air*, 2016, 26, 702–713.

9 6 S. Thepanondh, J. Varoonphan, P. Sarutichart and T. Makkasap, *Water. Air. Soil Pollut.*, 2011, 214, 83–
10 92.

11 7 M. L. Sattler and H. M. Liljestrand, *J. Air Waste Manag. Assoc.*, 2003, 53, 3–12.

12 8 L. Zhong, F. Haghghat, P. Blondeau and J. Kozinski, *Build. Environ.*, 2010, 45, 2689–2697.

13 9 L. Zhong and F. Haghghat, *Build. Environ.*, 2015, 91, 191–203.

14 10 J. Zhao and X. Yang, *Build. Environ.*, 2003, 38, 645–654.

15 11 INRS, *Benzène, Fiche toxicologique n°49*, 2009.

16 12 INRS, *Toluène, Fiche toxicologique n°74*, 2012.

17 13 INRS, *Ethylbenzène, Fiche toxicologique n°266*, 2018.

18 14 INRS, *Xylènes, Fiche toxicologique n°77*, 2009.

19 15 J. Morin, A. Gandolfo, B. Temime-Roussel, G. Brochard, V. Bergé, S. Gligorovski and H. Wortham,
20 *Build. Environ.*, 2020, 179, 106979.

21 16 S. Hazrati, R. Rostami, M. Farjaminezhad and M. Fazlzadeh, *Atmos. Environ.*, 2016, 132, 91–97.

22 17 J. Morin, A. Gandolfo, B. Temime-Roussel, R. Strekowski, G. Brochard, V. Bergé, S. Gligorovski and H.
23 Wortham, *Build. Environ.*, 2019, 156, 225–232.

24 18 J. Auvinen and L. Wirtanen, *Atmos. Environ.*, 2008, 42, 4101–4112.

25 19 A. Gandolfo, S. Marque, B. Temime-Roussel, R. Gemayel, H. Wortham, D. Truffier-Boutry, V.
26 Bartolomei and S. Gligorovski, *Environ. Sci. Technol.*, 2018, 52, 11328–11337.

27 20 T. Salthammer and F. Fuhrmann, *Environ. Sci. Technol.*, 2007, 41, 6573–6578.

28 21 A. Rosset, V. Bartolomei, J. Laisney, N. Shandilya, H. Voisin, J. Morin, I. Michaud-Soret, I. Capron, H.
29 Wortham, G. Brochard, V. Bergé, M. Carriere, F. Dussert, O. Le Bihan, C. Dutouquet, A. Benayad, D.
30 Truffier-Boutry, S. Clavaguera and S. Artous, *Env. Sci Nano*, 2021, 8, 758–772.

31 22 V. Bartolomei, M. Sörgel, S. Gligorovski, E. G. Alvarez, A. Gandolfo, R. Strekowski, E. Quivet, A. Held,
32 C. Zetzsch and H. Wortham, *Environ. Sci. Pollut. Res.*, 2014, 21, 9259–9269.

33 23 A. Manoukian, E. Quivet, B. Temime-Roussel, M. Nicolas, F. Maupetit and H. Wortham, *Environ. Sci.*
34 *Pollut. Res.*, 2013, 20, 4659–4670.

35 24 T. G. Karl, T. J. Christian, R. J. Yokelson, P. Artaxo, W. M. Hao and A. Guenther, *Atmospheric Chem.*
36 *Phys.*, 2007, 7, 5883–5897.

37 25 J. A. de Gouw, P. D. Goldan, C. Warneke, W. C. Kuster, J. M. Roberts, M. Marchewka, S. B. Bertman, A.
38 A. P. Pszenny and W. C. Keene, *J. Geophys. Res. Atmospheres*, DOI:10.1029/2003JD003863.

39 26 B. T. Jobson, M. L. Alexander, G. D. Maupin and G. G. Muntean, *Int. J. Mass Spectrom.*, 2005, 245, 78–
40 89.

41 27 E. von Hartungen, A. Wisthaler, T. Mikoviny, D. Jaksch, E. Boscaini, P. J. Dunphy and T. D. Märk, *Int. J.*
42 *Mass Spectrom.*, 2004, 239, 243–248.

43 28 A. Gandolfo, V. Bartolomei, E. Gomez Alvarez, S. Tlili, S. Gligorovski, J. Kleffmann and H. Wortham,
44 *Appl. Catal. B Environ.*, DOI:10.1016/j.apcatb.2014.11.011.

45 29 ISO 16474-3: 2013, 2013.

46 30 D. Truffier-Boutry, B. Fiorentino, V. Bartolomei, R. Soulas, O. Sicardy, A. Benayad, J.-F. Damlencourt,
47 B. Pépin-Donat, C. Lombard, A. Gandolfo, H. Wortham, G. Brochard, A. Audemard, L. Porcar, G. Gebel
48 and S. Gligorovski, *Environ. Sci. Nano*, 2017, 4, 1998–2009.

49 31 B. J. Finlayson-Pitts and J. N. Pitts, *Chemistry of the upper and lower atmosphere : theory,*
50 *experiments, and applications*, Academic Press, 2000.

51 32 Y. Bedjanian and A. El Zein, *J. Phys. Chem. A*, 2012, 116, 1758–1764.

- 1 33 W. Behnke, C. George, V. Scheer and C. Zetzsch, *J. Geophys. Res. Atmospheres*, 1997, 102, 3795–
2 3804.
- 3 34 D. O. Cooney, S.-S. Kim and E. James Davis, *Chem. Eng. Sci.*, 1974, 29, 1731–1738.
- 4 35 A. Hansel, A. Jordan, R. Holzinger, P. Prazeller, W. Vogel and W. Lindinger, *Int. J. Mass Spectrom. Ion*
5 *Process.*, 1995, 149, 609–619.
- 6 36 W. Lindinger, A. Hansel and A. Jordan, *Int. J. Mass Spectrom. Ion Process.*, 1998, 173, 191–241.
- 7 37 A. Fujishima, T. N. Rao and D. A. Tryk, *J. Photochem. Photobiol. C Photochem. Rev.*, 2000, 1, 1–21.
- 8 38 O. Geiss, C. Cacho, J. Barrero-Moreno and D. Kotzias, *Build. Environ.*, 2012, 48, 107–112.
- 9 39 W. Yu, M. in 't Veld, R. Bossi, M. Ateia, D. Tobler, A. Feilberg, N. Bovet and M. S. Johnson,
10 *Sustainability*, 2021, 13, 4821.
- 11 40 J. Chen and C. Poon, *Build. Environ.*, 2009, 44, 1899–1906.
- 12 41 T. Maggos, J. G. Bartzis, P. Leva and D. Kotzias, *Appl. Phys. A*, 2007, 89, 81–84.
- 13 42 R. A. R. Monteiro, F. V. S. Lopes, A. M. T. Silva, J. Ângelo, G. V Silva, A. M. Mendes, R. A. R. Boaventura
14 and V. J. P. Vilar, *Appl. Catal. B Environ.*, 2014, 147, 988–999.
- 15 43 P. Pichat, *Appl. Catal. B Environ.*, 2010, 99, 428–434.
- 16 44 S. Pal, V. Contaldi, A. Licciulli and F. Marzo, *Coatings*, , DOI:10.3390/coatings6040048.
- 17 45 T. Martinez, A. Bertron, G. Escadeillas, E. Ringot and V. Simon, *Build. Environ.*, 2014, 71, 186–192.
- 18 46 J. Laisney, A. Rosset, V. Bartolomei, D. Predoi, D. Truffier-Boutry, S. Artous, V. Bergé, G. Brochard and
19 I. Michaud-Soret, *Env. Sci Nano*, 2021, 8, 297–310.
- 20